Characterization of Sunshine Duration in Western Equatorial Africa: In Situ Measurements versus SARAH-2 Satellite Estimates

Nathalie Philippon, Amine Ouhechou, Pierre Camberlin, J. Trentmann, A. H.
Fink, J.D. Maloba Makanga, Béatrice Morel, G. Samba

HAL Id: hal-03695901

https://hal.univ-reunion.fr/hal-03695901

Submitted on 6 Oct 2022

Characterization of Sunshine Duration in Western Equatorial Africa: In Situ Measurements versus SARAH-2 Satellite Estimates✎

N. PHILIPPON,[a] A. OUHECHOU,[a] P. CAMBERLIN,[b] J. TRENTMANN,[c] A. H. FINK,[d] J. D. MALOBA,[e] B. MOREL,[f] AND G. SAMBA[g]

[a] *Institut des Géosciences de l'Environnement, Université Grenoble Alpes, CNRS, IRD, Grenoble INP, Grenoble, France*
[b] *Centre de Recherches de Climatologie, UMR 6282 Biogéosciences, CNRS/Université de Bourgogne Franche-Comté, Dijon, France*
[c] *Deutscher Wetterdienst, Offenbach, Germany*
[d] *Institute of Meteorology and Climate Research, Karlsruhe Institute of Technology, Karlsruhe, Germany*
[e] *Laboratoire d'Analyse Spatiale et des Environnements Tropicaux, Université Omar Bongo, Libreville, Gabon*
[f] *Laboratoire d'Energétique, d'Electronique et Procédés–Energy Lab, Université de La Réunion, Saint Denis, France*
[g] *Centre de Recherche et d'Etude sur l'Environnement, Ecole Normale Supérieure, Université Marien Ngouabi, Brazzaville, Republic of the Congo*

ABSTRACT: Western Equatorial Africa is one of the least sunny areas in the world. Yet, this has attracted little research so far. As in many other parts of Africa, light availability is mainly estimated using in situ measurements of sunshine duration (SDU). Therefore, this study conducts the first characterization of SDU evolution during the annual cycle for the region. It also evaluates the skill of satellite-based estimates of SDU from the Surface Solar Radiation Data Set–Heliosat, edition 2.1 (SARAH-2.1). Mean annual SDU levels are low: less than 5 h day^{-1} at the regional scale, with the sunniest stations in the northeast (Cameroon and Central African Republic) and the least sunny in an ~150-km-wide coastal strip in Gabon and Republic of the Congo (RoC). For most of the stations except the southeast ones in the Democratic Republic of Congo, the lowest SDU levels are recorded in July–September, during the main dry season, with persistent overcast conditions. They are as low as 2.5 h day^{-1}, especially on the windward slopes of the Massifs du Chaillu and du Mayombé, and of the Batéké Plateaus in Gabon and RoC. Although the mean annual and monthly spatial patterns are well reproduced in SARAH-2.1, SDU levels are systematically overestimated by 1–2 h day^{-1}. The largest positive biases are recorded during the December–February dry season, especially at the northernmost stations. Analyses at the daily time scale show that SARAH-2.1 biases arise from a twofold problem: the number of dark days (SDU < 1 h day^{-1}) is 50% lower than observed whereas that of sunny days (SDU > 9 h day^{-1}) is 50% higher than observed.

KEYWORDS: Africa; Bias; Climatology; Cloud cover; Shortwave radiation; In situ atmospheric observations; Satellite observations; Seasonal cycle; Local effects; Clustering

---

1. Introduction

Solar radiation is a key component for climate and ecosystems functioning and is relevant for many applications such as in the fields of energy, agronomy, hydrology. In the energy field, the seventh goal of the Sustainable Development Goals of the United Nations (https://sdgs.un.org/goals), which aims at ensuring access to affordable, reliable, sustainable, and modern energy for all by 2030, implies a shift away from fossil-fuel-based sources toward renewable energy sources (e.g., Gielen et al. 2019). Both photovoltaic (PV) and concentrated solar power (CSP) systems rely on solar radiation measures and estimates and would be promising solutions for sustainable power production (Neher et al. 2020; Hagumimana et al. 2021), especially in sub-Saharan Africa where more than one-half of the people still lack access to electricity (e.g., Quansah et al. 2016).

In the agronomic field, solar radiation is known to control and play on several parameters critical for plant growth and crop yields. For example, with regard to phenology, solar radiation and photoperiodism have been recently shown to be the main controlling factors of crops growth periodicity in Africa (onset, end, Adole et al. 2019; flowering, Upadhyaya et al. 2021). The evergreen forests functioning is also tightly related to solar radiation (Yang et al. 2021). This is especially true in Amazonia where mean annual variations in light availability have been shown to be the governing factor for photosynthesis (Huete et al. 2006; Myneni et al. 2007; Wagner et al. 2017): the sunny dry season sustains the highest photosynthesis levels.

The picture is different for central Africa forests. First, because mean annual rainfall is much lower, forests photosynthesis is primarily tied to water availability (Guan et al. 2015). The mean seasonal cycle of photosynthesis is in phase with that of rainfall: both are bimodal with two maxima in March–May and September–November (Gond et al. 2013). At the interannual time scale, anomalously low rainfall amounts during key periods of the seasonal cycle have been shown to lead
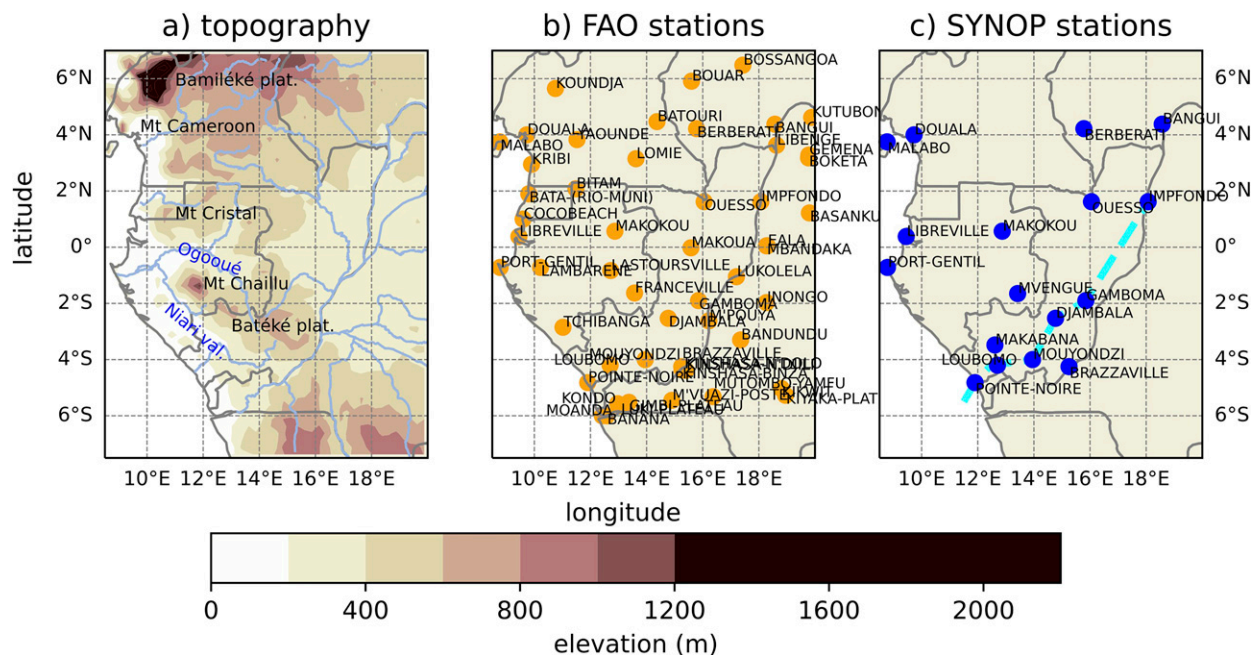

FIG. 1. (a) Topography, and location of the stations extracted for WEA from (b) FAO and (c) SYNOP databases. There are 53 FAO and 17 SYNOP stations. In (c), the dashed cyan line indicates the southwest–northeast transect that was analyzed.

to decline in forest greenness (Zhou et al. 2014). Second, the seasonality and quantity of light available for forests in central Africa are different from those in Amazonia. The highest light levels are recorded during the rainy seasons (Philippon et al. 2016; Bush et al. 2020) and not during the dry seasons. Moreover, the dense forests of western equatorial Africa (WEA) grow under particularly low light levels (Philippon et al. 2019) mainly because the main dry season is characterized by overcast skies (Dommo et al. 2018).

In WEA as in many other parts of Africa, measurements of incoming global solar radiation are infrequent. Pyranometers are rarely installed at synoptic weather stations. Most stations are equipped with the relatively cheap and easy to maintain Campbell–Stokes sunshine recorders that provide sunshine duration records (SDU). Actually, SDU is the measured characteristic of solar radiation with the longest records, thus yielding the most robust results with respect to the mean sunshine climatologies and long-term variability. However, time series length does not compensate for coarse spatial cover. Thus, to get an as accurate spatial picture as possible of light availability in WEA forests, it is necessary to rely on satellite products. Most of them, though, provide estimates of solar radiation and not SDU. Interestingly, the EUMETSAT Satellite Application Facility on Climate Monitoring (CMSAF) has recently issued a 35-yr record of SDU estimates for the Africa–Europe zone from Meteosat within the Surface Solar Radiation Data Set–Heliosat, edition 2.1 (SARAH-2.1), product.

Therefore, the objective of this study is twofold: 1) to characterize sunshine duration in WEA—actually, this is one of the areas in the world with the least sunshine, yet this has attracted surprisingly little research so far—and 2) to assess the reliability and accuracy of SARAH-2.1 SDU estimates

against in situ measurements from two independent databases—the Food and Agriculture Organization (FAO) archives and the synoptic (SYNOP) weather observations.

The main questions we intend to answer are the following: what are the observed levels of sunshine duration across WEA? How do they vary along the annual cycle? What are the physical factors explaining these variations? How good is SARAH-2.1 at reproducing the mean spatial patterns and seasonal evolution of SDU as compared with in situ measurements?

The study is organized into four sections: Section 2 describes the three SDU databases used, namely, SARAH-2.1, FAO, and SYNOP. Methods used to characterize SDU mean space–time variations, and to assess SARAH-2.1 accuracy versus surface measurements are also presented. Results are provided in section 3. SDU mean annual patterns and monthly evolutions are first discussed. A division of WEA into characteristic areas based on SDU mean seasonal cycles is provided. The dependence of SDU mean spatial patterns on topography is also assessed. Then the accuracy of SARAH-2.1 SDU estimates at the daily time scale is evaluated with a focus put on the June–September overcast dry season. Links with cloudiness are also explored. Section 4 closes the paper by discussing and summarizing the findings.

2. Data and methods

In the present study, the focus is put on WEA, defined as the region located between latitudes 8°S and 7°N and between longitudes 8° and 20°E (Fig. 1a). It comprises southern Cameroon, Equatorial Guinea, Gabon, the Republic of the Congo (RoC), the southwestern Central African Republic (CAR), and the western Democratic Republic of Congo

(DRC). We jointly analyze three independent databases of SDU: CMSAF SARAH-2.1 satellite estimates and in situ measurements extracted from the FAO database and from SYNOP reports. Only pixels and stations located within WEA were extracted from the three databases. We selected the closest SARAH-2.1 pixels to the respective FAO and SYNOP stations. The main characteristics of these databases are described below.

a. CMSAF SARAH-2.1 sunshine duration estimates

The CMSAF SARAH-2.1 climate data record (referred to as SARAH-2 herein), provides subdaily, daily, and monthly records for Europe and Africa of six solar radiation related parameters among which are daily and monthly sunshine durations. Records cover the 35-yr period 1983–2017 with a 0.05° latitude–longitude resolution and are derived from measurements from the Meteosat Visible and Infrared Imager (MVIRI) and Spinning Enhanced Visible and Infrared Imager (SEVIRI) instruments on board the geostationary *Meteosat-2–Meteosat-10* satellites. SDU estimations are based on the direct normalized irradiance (DNI) estimates. The WMO threshold for bright sunshine is defined as DNI $\geq$ 120 W m^{-2}. Daily SDU is computed as the ratio of Meteosat daylight slots with DNI exceeding the WMO threshold to all potential daylight slots, multiplied by the day length. Details on the computation of SDU and in particular on the weighting applied to slots as a function of the surrounding grid points can be found in Kothe et al. (2017).

b. Sunshine duration in situ measurements from the FAO database

The Food and Agriculture Organization has compiled a global agroclimatic database called FAOCLIM2 (http://www.fao.org/nr/climpag/pub/en1102_en.asp) that contains long-term monthly averages at ~28 800 stations for up to 14 climatic variables including SDU. We have extracted from FAOCLIM2 long-term SDU monthly averages for 53 stations in WEA, that is, 12 monthly SDU values per station. The location of the 53 stations is given in Fig. 1b as orange dots. These long-term monthly averages are computed over time periods that vary across stations but are generally within the period 1951–90.

To ensure the reliability of these long-term monthly averages, a quality check of FAO data against independent sources for a few stations has been performed (see the online supplemental material). These include unpublished records from RoC meteorological services and long-term monthly means from a variety of publications (references provided in the online supplemental material). At Douala (Cameroon), old and more recent records show very large discrepancies, associated with a documented shift of the station location possibly combined with a change in the recording instruments. At Bangui (CAR), Callède and Arquisou (1972) found that old sunshine records, based on unknown instruments, were underestimating SDU relative to measurements made using Campbell–Stokes heliographs. A similar change of instruments at Douala may then explain the higher SDU values published as 1961–90 climatological normals (WMO 1998) relative to 1931–60 normals (WMO 1969), the latter being

retained in the FAO database. A few other cases of poor agreement between the different sources [e.g., at Port-Gentil (Gabon)] remain of unknown origin. On the whole however, the comparison reveals a relatively good agreement between FAO data and other sources at most stations, with discrepancies seemingly due to the length of records available and the differing periods. The FAO database was, therefore, used as is, with the exception of the station of Dolisie (RoC), which has been removed because of unreliable data, while for the station of Pointe Noire (RoC) the inconsistent value for December, that is, 0 h day^{-1}, has been replaced by the annual mean, which equals 4.1 h day^{-1}. This is consistent with the mean value obtained from the "OGIMET" database (see section 2c) for December and the period 1999–2018 and that equals 4.25 h day^{-1}.

c. Sunshine duration and cloud cover in situ measurements from SYNOP reports

SYNOP reports issued from national meteorological agencies and collected via WMO's Global Telecommunication System, were extracted from the OGIMET database (http://www.ogimet.com/index.phtml.en). For our study purposes, we extracted daily SDU and 3-hourly cloud-cover (both total and low cloud cover) data for 17 stations across WEA (Fig. 1c, blue dots). The period covered is 1999–2018. SDU values are given in hour per day. Cloud-cover data are in octas, ranging from 0 for clear skies to 8 for totally overcast skies. To enable comparisons with SDU, only daytime cloud-cover records (from 0600 to 1800 UTC) were considered, and a daily average was computed only if at least 3 of 5 three-hourly records were available.

The best documented stations among the 17 stations available are Pointe Noire, Brazzaville (RoC), Douala, Bangui, Libreville (Gabon), and Port-Gentil. The least documented ones are Gamboma (RoC), Impfondo (RoC), and Makokou (Gabon) (Fig. S1 in the online supplemental material). Note also that there are only 15 stations common to both FAO and SYNOP databases.

d. Dataset comparison and measures of skill

Given the time resolution of the databases studied, SYNOP reports were compared with SARAH-2 in terms of both mean annual cycles and the daily variations. Additionally, SDU mean annual cycles were compared between SARAH-2 and FAO data. Note also that we did not work with the relative sunshine duration, that is, SDU divided by day length, because in the equatorial band the length of daylight undergoes very little variation over the year: the largest differences in the daylight length between the northernmost and southernmost stations studied [i.e., Bossangoa (CAR) and Muanda (DRC)] are observed at the two solstices and do not exceed 45 min.

To determine SARAH-2's accuracy at estimating SDU for WEA, a variety of measures was applied. First, Pearson correlation coefficient (and the corresponding p values) and biases (difference between SARAH-2 and in situ SDU values) were computed. The aim is to assess the spatial and temporal matches and point out over or underestimations in SARAH-2

TABLE 1. Example of contingency table for assessing SARAH-2 skills to detect either dark (25th percentile) or bright (75th percentile) days.

		In situ (SYNOP)	
		≤25% (≥75%)	>25% (<75%)
SARAH-2	≤25% (≥75%)	Hits (H)	False alarms (FA)
	>25% (<75%)	Misses (M)	Correct negatives (CN)

estimates as compared with in situ measurements for specific areas or seasons. These measures are especially used when dealing with mean annual and mean monthly SDU levels. Second, we also applied metrics usually used for forecasts verifications (Wilks 2011) but also for satellite estimates and models performance assessment (e.g., Amjad et al. 2020; Maranan et al. 2018): the probability of detection (POD), the false alarm ratio (FAR), and the Heidke skill score (HSS). These measures are applied when analyzing SDU at the daily time scale. Indeed, at this time scale, daily SDU levels do not follow a normal distribution (cf. section 4c), so Pearson correlations and biases are less appropriate. Second, POD, FAR, and HSS, which are categorical skill scores, are less sensitive to bias.

POD and FAR are computed for "dark days" (least sunny) and "bright days" (sunniest) separately. Dark days are defined as days recording SDU values below the 25th percentile. Bright days are those recording SDU values above the 75th percentile. Two 2-dimensional contingency tables are issued: one for the dark days where SDU raw values are categorized according to the 25th percentile, and one for the bright days where SDU raw values are categorized according to the 75th percentile. Table 1 provides an example of such contingency tables.

POD corresponds to the fraction of bright (or dark) days observed at the stations and correctly detected in SARAH-2 [i.e., $POD = H/(H + M)$ in Table 1]. A perfect score is equal to 1. Complementarily, FAR is the fraction of bright (dark) days (i.e., 25th > day > 75th percentile) incorrectly detected by SARAH-2, that is, not observed at the stations [i.e., $FAR = FA/(H + FA)$ in Table 1]. A perfect score is 0. Last, HSS is a measure of accuracy relative to that of chance. $HSS = (H + CN - e)/(CN - e)$, where e is the correct random forecasts. A perfect score is 1; a score of 0 indicates no skill. Note that, unlike POD and FAR, HSS is not defined separately for dark and bright days but rather from a three-dimensional contingency table.

e. Clustering of the mean annual cycles

The k-means clustering analyses applied here have two objectives: (i) discriminate subregions within WEA according to the shape and amplitude of the mean annual cycle and (ii) verify SARAH-2 capabilities. Two different approaches have been tested: 1) a k-means clustering of FAO SDU data followed by projections of the clusters onto SARAH-2 SDU data, and 2) two k-means clustering analyses independently

applied to FAO and SARAH-2 SDU data. Only the results from this latter approach were retained because with the former one the cluster that depicts the least sunny stations does not show up in SARAH-2 because of the systematic overestimation of SDU in this product.

A solution with four clusters was retained as optimal with coherent and sounding spatial patterns and the highest silhouette coefficient. This coefficient was computed using the mean intracluster distance and the mean nearest-cluster distance. It varies between −1 and 1, with 0 indicating overlapping clusters and negative values indicating an assignment to a wrong cluster.

3. Results

a. Mean annual spatial distribution of sunshine duration across WEA

The mean annual fields of SDU as depicted from SARAH-2 satellite estimates, and FAO and SYNOP surface measurements are provided in Fig. 2. First, annual SDU levels are very low: on average they do not exceed 6.7 h day^{-1} for SARAH-2 (FAO: 5.2 h day^{-1}; SYNOP: 4.8 h day^{-1}), ranging from 1.4 or 3.2 h day^{-1} for the least sunny pixels or station, respectively, to 10.6 or 7.7 h day^{-1} for the sunniest pixels or station, respectively. Second, although computed at different time periods, the spatial patterns of SDU are in good agreement among the three databases. The least sunny places are in the vicinity of the Cameroon volcanic ridge (e.g., Douala, Malabo), of the Monts de Cristal and Nyanga Valley (e.g., Tchibanga) in Gabon, and extend to the south of RoC (Loubomo) and DRC (Kondo, Luki, and Gimbi Plateau). Their mean annual SDU is below 5 h day^{-1} in SARAH-2 and below 4 h day^{-1} in FAO and SYNOP. From this band of low SDU somewhat parallel to the Atlantic Ocean coast, durations gradually increase inland. Satellite estimates also show that SDU increases offshore and is thus higher over the ocean.

Figures 3a–c presents scatterplots between the mean SDU annual values of the three databases taken two by two: FAO against SYNOP, SARAH-2 against FAO, and SARAH-2 against SYNOP. The agreement between the 15 stations common to the two surface databases (FAO and SYNOP, Fig. 3a) is good. The correlation coefficient reaches 0.86 suggesting that the spatial distribution of SDU is comparable between the two databases. The mean regional bias is weakly positive (0.2 h day^{-1}), indicating that SDU levels are slightly higher in SYNOP, especially for the sunniest stations as suggested by the slope of the regression line. Scatterplots for SARAH-2 against FAO or SYNOP and the respective correlation coefficients confirm that the spatial distribution of SDU mean annual values is well captured by SARAH-2. However, the large positive biases (~1.4 h day^{-1}) indicate that SARAH-2 strongly overestimates SDU levels for WEA. The slope of the regression lines suggests that the less sunny the station, the larger the biases.

Maps of raw biases (Figs. 3d–f) do not exhibit any particular spatial pattern. Some stations in Cameroon display biases above 2.5 h day^{-1}, reaching ~3 h day^{-1} at Douala and Bitam. Douala's large bias may be attributed to the uncertain reliability of the FAO record, as discussed previously. However,
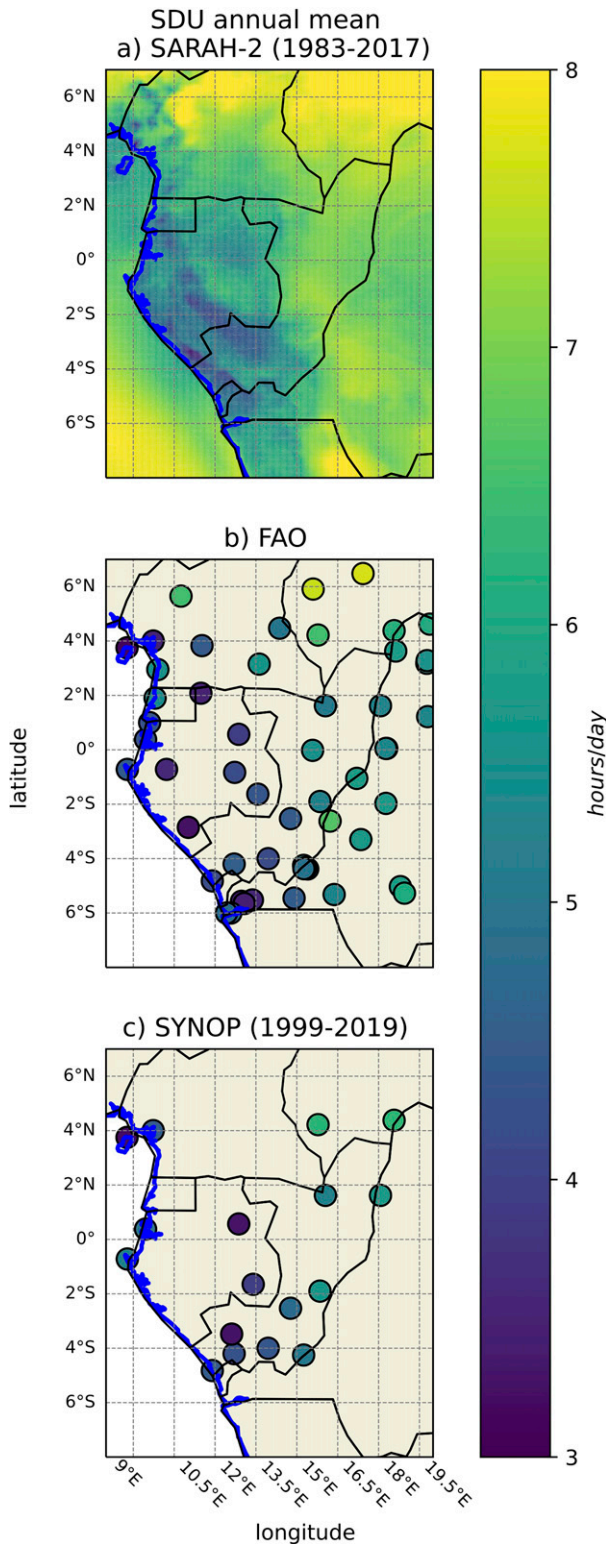
FIG. 2. SDU mean annual fields for (a) SARAH-2, (b) FAO, and (c) SYNOP.

it can be seen in Figs. 3g–i that stations at or close to the coast that are also the less sunny, tend to have higher relative biases (above 50%).

b. Seasonal evolution of sunshine duration

1) SARAH-2 SKILL AND BIASES ALONG THE ANNUAL CYCLE

The mean spatial distribution of SDU in WEA for the representative months of January, April, July, and October and the three databases is displayed in Fig. 4. In SARAH-2 (Fig. 4, top panels) the highest SDU levels (>6 h day^{-1}) are observed in January, during the boreal dry season, with maxima in the northern part of the study region. The lowest levels (<5 h day^{-1}) are recorded in July, during the austral dry season, except for a band stretching from the center of RoC to the north of Angola where levels are the highest of the year. This band encompasses the western escarpment and the summit of the Batéké Plateau characterized by an encroachment of savanna in the rain forest (Verhegghen et al. 2012). At the coast and within a ~150-km-wide band inland, SDU levels are particularly low: less than 3 h day^{-1}. The months of April and October correspond to the core of the two rainy seasons. However, SDU levels are not as low as in July, during the austral dry season, a typical feature of WEA (Philippon et al. 2016; Bush et al. 2020). April is slightly sunnier than October but not as sunny as January.

The spatial match between SARAH-2 and FAO-SYNOP in the course of the annual cycle is further assessed through monthly scatterplots presented in Fig. 5. First, scatterplots clearly display the evolution in the range of SDU levels along the annual cycle: the March–May rainy season is the one when spatial differences in SDU mean levels are the smallest (<4 h day^{-1}) across WEA as opposed to the June–August dry season (>6 h day^{-1}). Second, the largest biases (>2 h day^{-1}) are in December–February, the boreal winter dry season, and the lowest are in May–June and September–October, that is, the transition months between the two rainy seasons and the austral winter dry season. The best spatial agreement (correlation coefficients ≥ 0.85), is observed in June–September (austral winter dry season) when SDU levels are the lowest, then in November–December. Last, the slope of regression lines also indicates that the agreement between SARAH-2 and in situ measurements is better at the sunniest stations.

The match between databases at station scale for the mean annual cycle is provided in Fig. 6 through correlation coefficients between the three databases taken two by two. In general terms, the best correspondence is observed for the northernmost and southernmost stations. This is related to the fact that SDU annual range is higher and that its seasonality is more pronounced at these stations. Discrepancies are larger for the Gabonese stations as well as the stations to the center and the north of RoC. SDU annual range is small at these stations and many RoC stations have short recording periods in SYNOP (Fig. S1 in the online supplemental
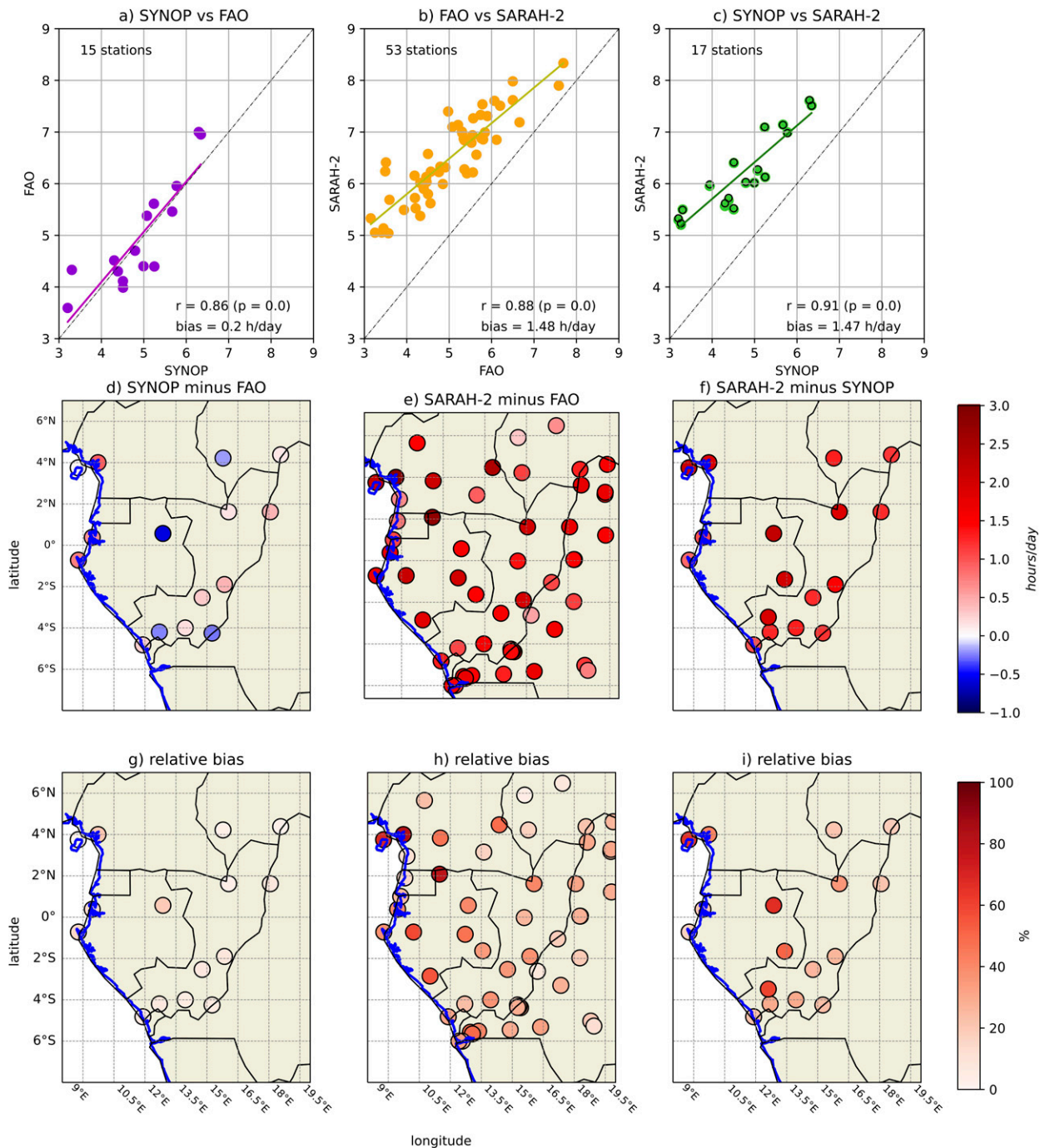
FIG. 3. Scatterplots and corresponding regression lines for SDU annual mean for (a) SYNOP against FAO, (b) FAO against SARAH-2, and (c) SYNOP against SARAH-2 (1 point = 1 pixel/station). The time period for computing the annual mean for SARAH-2 is 1983–2017 in (b) and 1999–2017 in (c) (black circles are for 1983–2017). The Pearson correlation coefficients (with their corresponding *p* values) and biases are annotated. Also shown aremaps of (middle) raw and (bottom) relative biases for (d),(g) SYNOP minus FAO; (e),(h) FAO minus SARAH-2; and (f),(i) SYNOP minus SARAH-2.

material). The bad fit for Brazzaville in SARAH-2 versus FAO or SYNOP in contrast to the good fit between FAO and SYNOP, suggests that the annual cycle inferred from SARAH-2 is wrong for this location.

Last, the SDU annual cycle from FAO, and the SARAH-2 biases with respect to FAO for the 53 stations ordered from north to south are presented in Fig. 7. Stations showing the largest seasonal variations are located in the north (highest
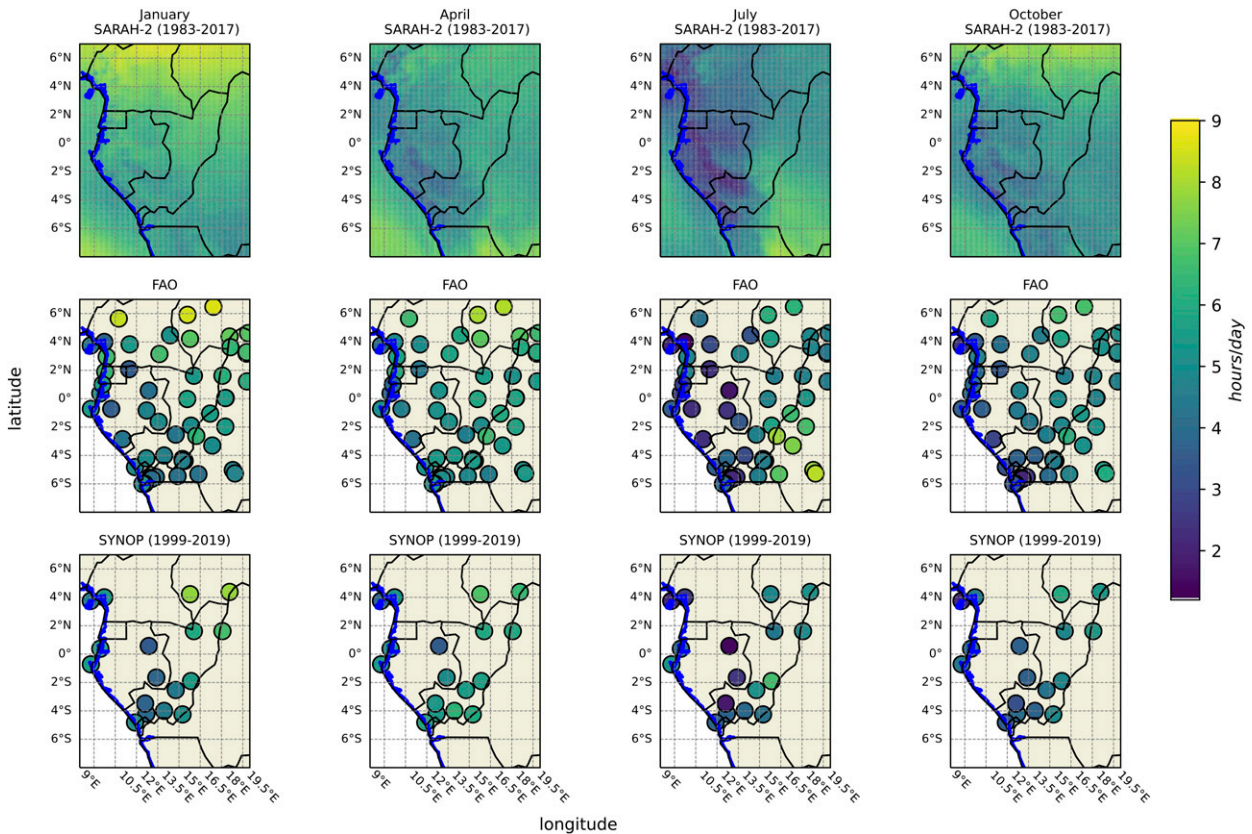
FIG. 4. (left) January, (left center) April, (right center) July, and (right) October SDU mean monthly fields for (top) SARAH-2, (middle) FAO, and (bottom) SYNOP.

SDU in boreal winter) and in the south (highest SDU in austral winter), but there are many stations where this pattern is substantially altered. These stations are characterized by very low SDU values in June–September (extending to October in the south), regardless of the latitude. They are all located in the western part of the region, along and close to the Atlantic Ocean. The southern part of the region is, therefore, remarkable by its strong contrasts in SDU annual cycles. In SARAH-2, biases are the largest (and positive) for the northernmost and southernmost stations and the boreal winter dry season (December–February). Apart from this, it is noteworthy that there is not any systematic bias especially for the least sunny stations and months.

2) REGIONALIZATION OF WEA BASED ON SDU MEAN ANNUAL CYCLE

Analyses developed in the above sections suggest that SARAH-2 reproduces well the spatial patterns of SDU mean seasonal evolution in WEA but is affected by large positive biases. They also suggest that differences exist between stations in the timing of minima and maxima during the annual cycle. These points are further explored through a distinction of WEA into subregions based on two k-means clusterings applied independently on FAO and SARAH-2 SDU mean annual cycles.

Results are provided in Fig. 8 with the spatial patterns displayed in Fig. 8a (with FAO stations as circles) and the corresponding annual cycles in Fig. 8b and Fig. 8c for FAO and SARAH-2, respectively. The clusterings discriminate first stations/pixels to the northeast ("trop. inland northeast," colored in orange, comprising CAR, N Cameroon, and DRC) and the southeast ("trop. inland southeast," colored in gray, comprising southern DRC), which are both tropical inland patterns but with reversed annual cycles: maxima are in December–January and June–July, and minima are in August and December, respectively. Second, it discriminates stations to the west ("coastal," colored in green, comprising southern Cameroon, Gabon, southwest RoC, and DRC) and the east ("equat. inland," colored in purple, comprising central RoC and DRC, as well as coastal Angola). These stations/pixels are characterized by (i) lower SDU levels than the tropical inland northeast and southeast, and (ii) maxima shifted to August–September. Despite their very different locations, the coastal and tropical inland northeast regions have remarkably similar annual cycles except that the coastal region has a much lower SDU, by 25%–50% in any month. Actually, besides differences in the annual mean SDU and amplitude of the annual cycle, the cluster's differentiation is mainly controlled by how much SDU differs in boreal summer from the rest of the year.
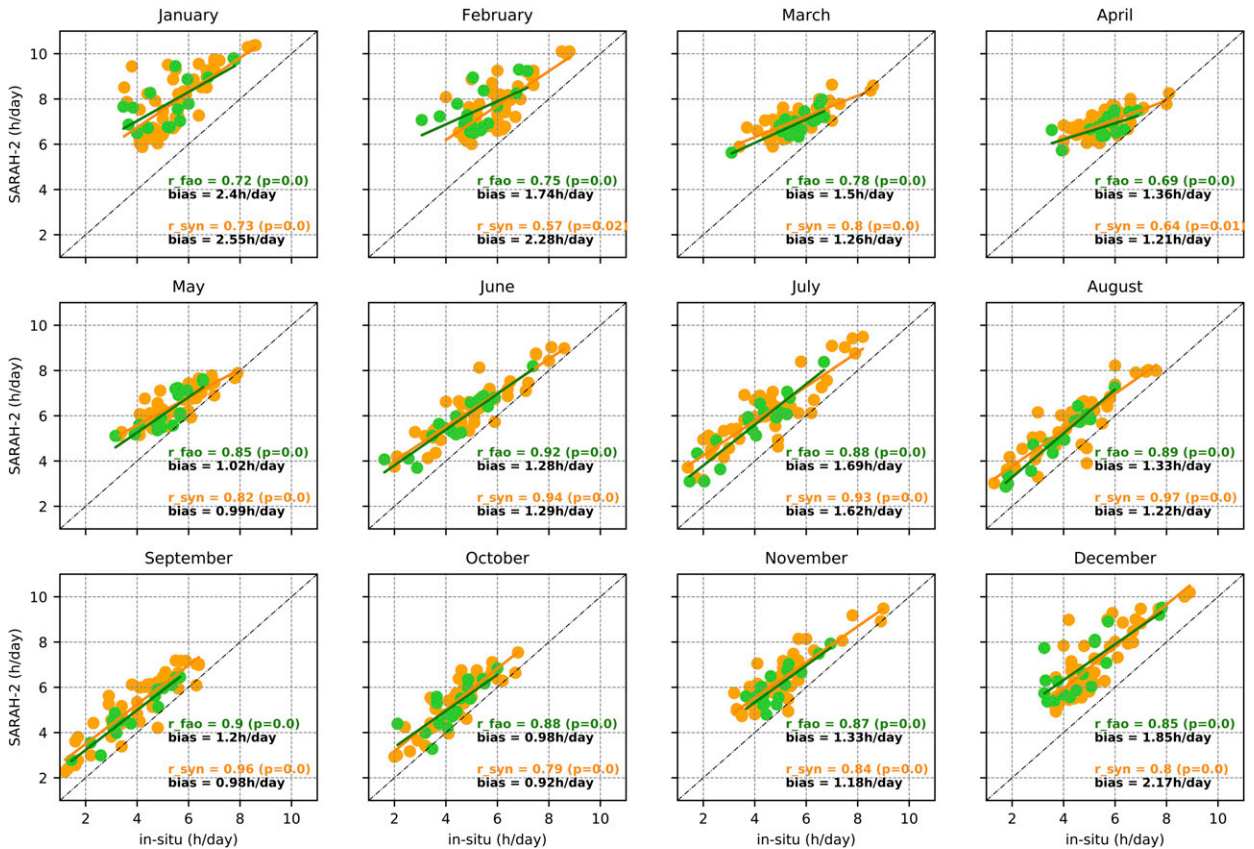
FIG. 5. Scatterplots and corresponding regression lines between SARAH-2 and FAO (orange) or SARAH-2 and SYNOP (green) SDU monthly means (1 point = 1 pixel/station). Regression lines, correlation coefficients (and their p values), and biases are annotated.

Last, it is noteworthy that the borders of the four regions extracted either from FAO or SARAH-2 match very well. Because of the positive biases in SARAH-2, the brightest region, that is, the tropical inland north (orange), is slightly moved southward as compared with FAO. Similarly, the least sunny region, that is, the coastal one (green) has a more restricted spatial extension toward the north and east as compared with FAO.
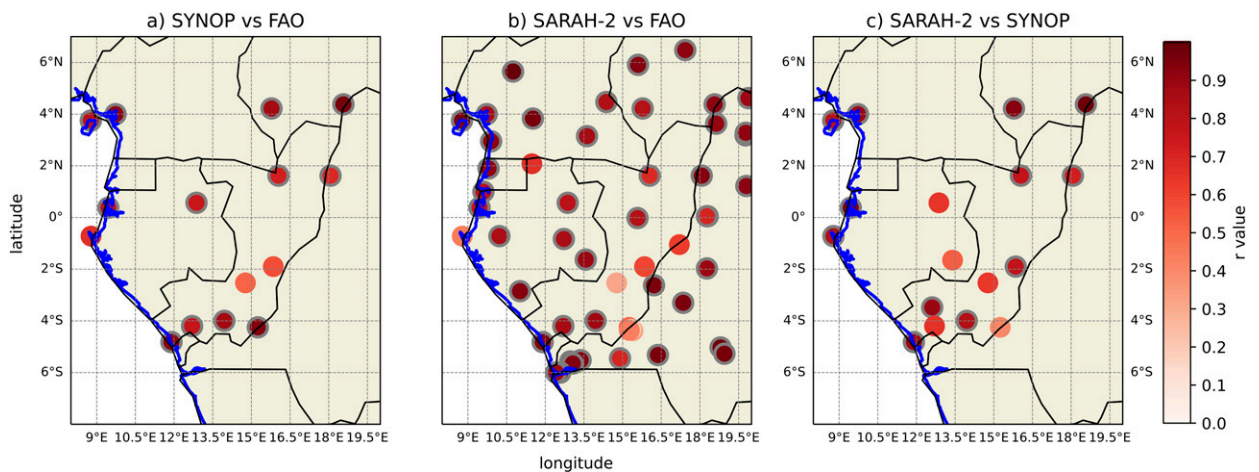

FIG. 6. Maps of the correlation coefficients between mean annual cycles for the three databases taken two by two. Gray-edged circles represent correlations that are significant at the 99% level.
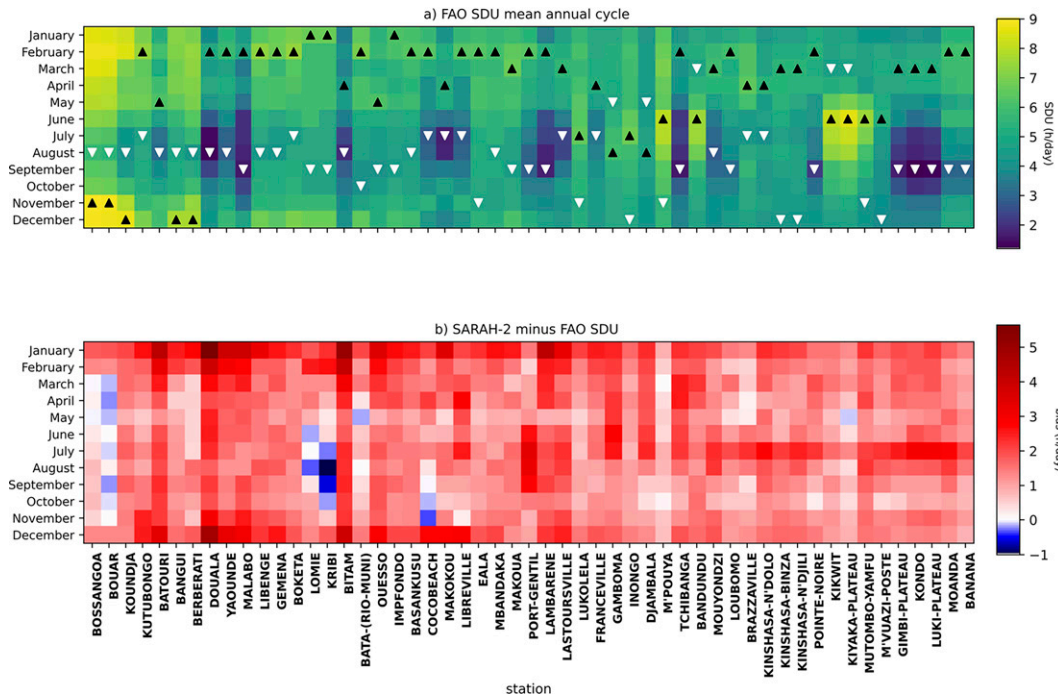
FIG. 7. Evolution along the annual cycle of (a) SDU in FAO and (b) raw biases in SARAH-2 vs FAO for each of the 53 available stations. Stations are ordered from the northernmost one to the southernmost one. In (a), black and white triangles respectively denote months of maximum and minimum SDU.

3) SDU'S MEAN SPATIAL DISTRIBUTION DEPENDENCE ON TOPOGRAPHY

While in Fig. 8 the delineations between clusters east of 15°E are relatively zonal, the inland boundary of the "coastal" region is complex, suggesting that local features have a major influence. WEA is characterized by a complex topography (Fig. 1) organized around several inland plateaus (Bamiléké in Cameroon, Batéké in RoC) and mountain ranges (Cristal and Chaillu in Gabon, Mayombé in RoC, and western DRC). With the exception of the volcanic peak of Mount Cameroon (4090 m) in the northwestern corner of the region, these mountains and plateaus are of low elevation: most of them culminate around 1000 m, but they are relatively parallel to the coastline. They are intersected by several valleys, for example, the upper Ogooué and Niari Valleys. Although there is a large coastal plain in Gabon at the mouth of the Ogooué, other coastal plains are relatively narrow (<100 km). To investigate the potential influence of topography on SDU spatial organization during the annual cycle, we used the USGS Shuttle Radar Topography Mission (SRTM) topographical data at 30 s resolution, regridded at 0.05° to match with SARAH-2.

Scatterplots (not shown) between SARAH-2 SDU mean monthly values and altitude do not depict any clear dependence of SDU on altitude. Similarly, spatial correlations computed between SDU and altitude over 2° square sliding windows for the 4 months of interest, that is, January, April, July, and October, picture inconsistent patterns (not shown). More interesting are the relationships with slope and aspect

provided in Fig. 9 and that focus on the regions south of the equator. SDU tends to be slightly higher on flat terrain in whatever month. In July and October, strong contrasts in SDU levels are pictured between the northeast (high SDU) and southwest-facing slopes (lower SDU). In July, differences in SDU mean levels between the two orientations exceed 2 h day^{-1} (the steepest the slope, the greatest the contrast). These contrasts might be explained by the dominant wind direction, the atmospheric stability, and the type of clouds in presence. In the eastern equatorial Atlantic and adjacent coastal areas, low-level winds are south-southwest throughout the year (Lacaux et al. 1992; Neupane 2016). Southwest-facing slopes might act as a barrier to the low-level winds, triggering cloudiness as the air mass is forced to uplift (which in turn strongly dampens the incoming solar radiation). However, the strong interaction found with topography in July (and somewhat in October) may be related to the fact that the lower troposphere is very stable at this time of the year while in the rest of the year it is much more unstable, resulting into widespread ascending motion (Cook and Vizy 2015; Longandjo and Rouault 2020). Even if the genesis of convective clouds may be impacted by interactions between low-level flow and topography, their subsequent drift in the direction of the easterly midtropospheric winds may blur any relationship with topography. In contrast, the low-level stratiform clouds that develop in June–September in a more laminar flow are likely less mobile than the convective clouds, so that their spatial spread is much more prone to be controlled by topography.
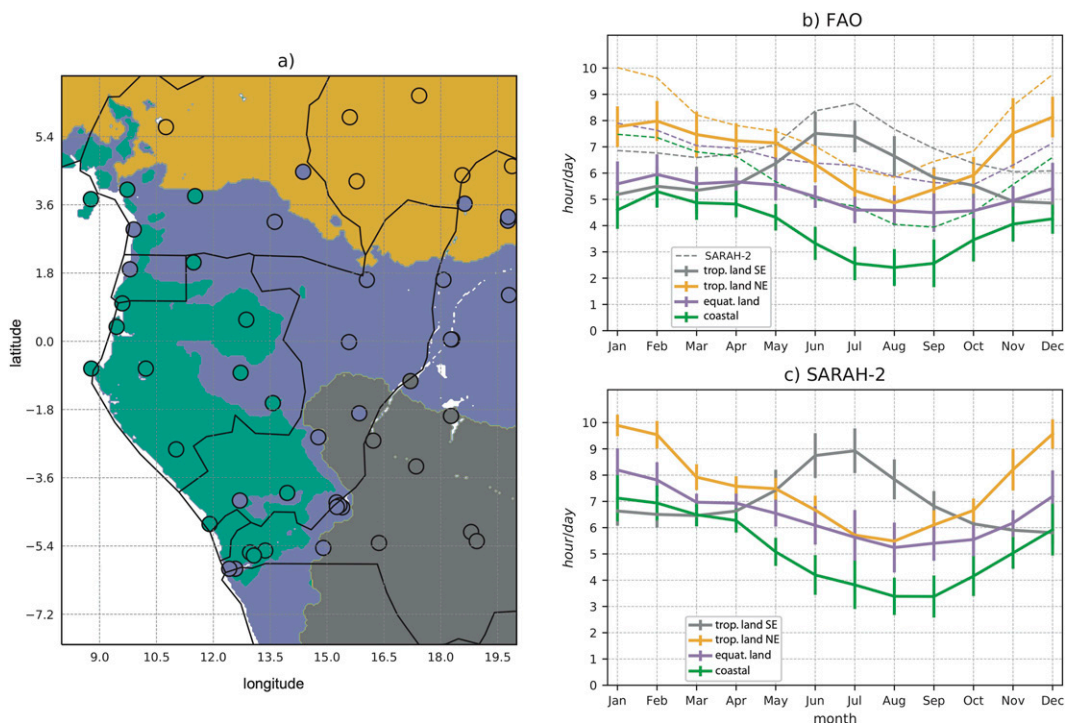
FIG. 8. Characteristic regions of SDU in WEA according to the mean annual cycles and based on *k*-means clustering analyses performed independently for FAO and SARAH-2. The solution with four clusters has been retained. (a) Location of the four classes, with FAO stations as circles and SARAH-2 pixels as colored fields. Also shown are the corresponding mean annual cycles for (b) FAO and (c) SARAH-2, with error bars for ±1 std dev. In (b), dashed lines give the SDU mean annual cycle computed from the SARAH-2 pixels corresponding to the FAO stations of the cluster.

To further document these contrasts linked to topography, SDU levels are plotted along a southwest–northeast cross section running through RoC, from the Atlantic coast at Pointe Noire (~12°E) to Impfondo (~18°E; cyan dashed line in Fig. 1) for the four months of interest (Fig. 10, upper panel, thick lines). This cross section intersects the Mayombé Massif and the Batéké Plateaus (Fig. 10, bottom panel). For validation purposes, SDU levels recorded at seven stations along the cross section are also reported. The influence of aspect on SDU is clearly the strongest in July. The orographic effect of Mayombé and Batéké Plateaus is obvious: their southwest-facing slopes record SDU levels much lower than their summits and east-facing slopes suggesting that cloudiness is larger on southwest-facing slopes. The sheltering effect of Batéké Plateaus is striking and coherent between SARAH-2 and in situ measurements despite the systematic bias. In October, the Mayombé coastal range still has an effect, but inland, while SDU remains low, topography does not seem to play a significant role any more. On the whole, SARAH-2 well captures SDU levels variations along the cross section and the annual cycle even if some discrepancies exist: in situ records suggest that SDU levels are higher in April than January in the western part of the transect, that is, on the southwest-facing slopes west of Djambala. This feature is not well captured by SARAH-2 where values are quite similar between the

two months. Conversely, SDU levels east of Djambala are higher in January than in April (they are constant in April), which is well depicted by SARAH-2. In situ records also suggest that SDU levels on southwest-facing slopes (Dimonika, Mouyondzi) are lower in July than in October. The reverse is observed in SARAH-2: SDU levels are lower in October than in July at these two locations.

c. SARAH-2 accuracy at the daily time scale: Focus on the austral winter dry season (June–September)

As SYNOP provides daily SDU records, this database is used to assess SARAH-2 accuracy at daily time scale. Only 16 couplets of "station–pixel" are available for analysis: Gamboma has been excluded because of too few data for the period 1999–2017 common to the two databases (Fig. S1 in the online supplemental material). In addition, missing dates in each database have been respectively masked in the other one. In this section a focus is put on the June–September dry season. This season pictures the lowest SDU levels over most of the SYNOP stations under analysis because of the presence of a large low-level cloud cover. It is also the season for which SARAH-2 biases are the lowest (cf. section 3b).

Figure 11 presents the distribution of SDU daily values for SARAH-2 and SYNOP considering the whole year (Fig. 11a) and the June–September season only (Fig. 11b). In WEA,
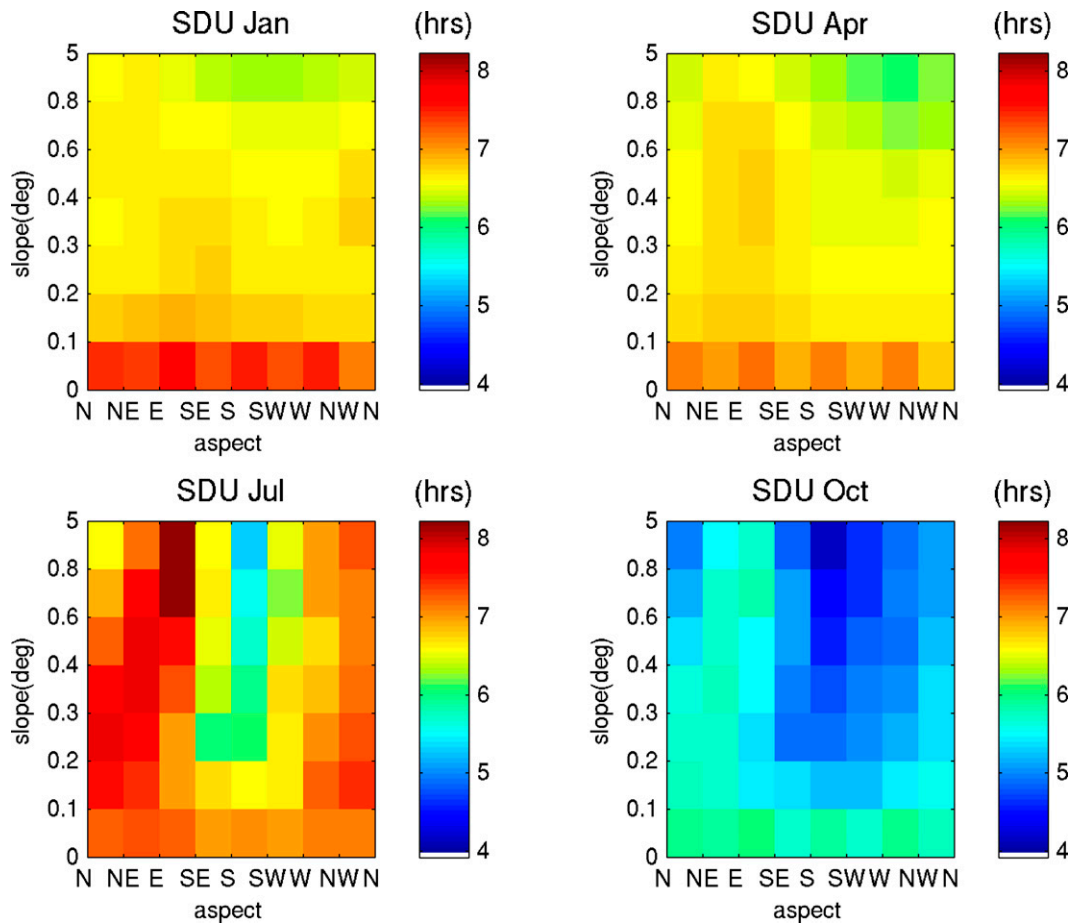
FIG. 9. Relationships between monthly SDU from SARAH-2 and slope and aspect from a digitalized elevation model for pixels south of the equator only. DEM values were regridded to SARAH-2 resolution. The mean SDU is given for each slope–aspect couple.

according to SYNOP the most frequent days are those recording less than 1h of sunshine. This is particularly so in June–September, the overcast dry season: the least sunny days (SDU < 1 h day^{-1}) account for 25% of the total number of days. In SARAH-2, the number of sunless days is 50% lower than in SYNOP. Reciprocally, there are more than twice as many days recording more than 9 h of sunshine in SARAH-2 as compared with SYNOP. This suggests that there are both too many clear-sky days and not enough totally overcast days in SARAH-2. Therefore, biases found in SARAH-2 at the annual and monthly time steps in the previous sections are linked to this twofold problem.

Given these large biases, SARAH-2 accuracy for properly estimating sunshine duration for a given day is evaluated using the categorical metrics POD, FAR, and HSS (cf. section 2d), in addition to the Pearson correlation coefficient. Scores obtained are presented in Fig. 12. The linear match at daily time scale between SARAH-2 and SYNOP (Figs. 12a,b) is globally good: at ~13 of 16 stations, correlations are above 0.75 (i.e., 56% of common variance at least). The HSS are > 0.4, at 6 stations of 15, namely, Douala, Port-Gentil,

Brazzaville, Pointe Noire, Bangui, Libreville (the best documented stations; Fig. S1 in the online supplemental material), indicating that SARAH-2 performs statistically much better than chance at identifying the least sunny and the sunniest days. Conversely, HSS are <0.1 at eight stations. For these stations SARAH-2 only performs slightly better than chance. This also suggests that, for these stations, correlations are driven by the skill for "average days" (i.e., days with SDU values between the 25th–75th percentiles). Stations with the lowest correlations and HSS scores are the Gabonese stations (noticeably, Mvengue and Makokou), those at the center and north RoC (Ouesso, Djambala) plus Malabo. POD scores are almost always >0.6; that is, more than 60% of the least sunny and sunniest days in SARAH-2 are actually the least sunny and sunniest days in SYNOP. FAR scores are almost always <0.3; that is, less than 30% of days detected as the least sunny and sunniest by SARAH were not so in SYNOP. Again Mvengue, Makokou, and Malabo stand out with low POD/high FAR scores, especially for the least sunny days. This is consistent with the low correlation and HSS scores obtained for these stations.
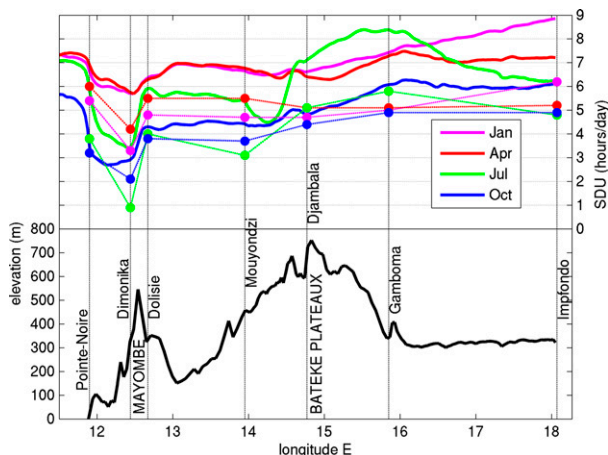
FIG. 10. Variations of (bottom) elevation and (top) SDU in WEA along a southwest–northeast cross section starting from Pointe-Noire and ending at Impfondo via the stations of Dimonika, Dolisie, Mouyondzi, Djambala, and Gamboma (see Fig. 1). In the top plot, there is one color for each of the four representative months of January, April, July, and October; thick lines are for SARAH-2 SDU, and dots are for FAO SDU at the given station.

As a last step, taking advantage of the cloud-cover data provided in SYNOP database, we briefly analyze relationships between SDU and cloud cover for the June–September overcast dry season only. The aim is to verify that the relationship observed in SYNOP is properly reproduced in SARAH-2. Results are provided in Fig. 13 considering the total cloud cover (TCC; left panels) and the low cloud cover only (LCC; right panels), and all the stations together (results for individual stations and LCC are provided in Fig. S2 of the online supplemental material).

First, SDU levels are globally well discriminated across classes of octas, with regularly decreasing SDU levels as cloud cover increases for both TCC and LCC. On average, in June–September (JJAS), clear-sky days (zero octa), which are rare (22 days in total), coincide with SDU levels around 8 h day^{-1}

according to SYNOP. To the contrary, totally overcast days (8 octas) are associated with SDU levels below 1 h day^{-1}. A few inconsistencies are nonetheless observed for the clearest days/skies. For the 1-octa class and LCC SDU levels are lower than or equal to SDU levels for the 2-octa class. These inconsistencies come from a few stations (Impfondo, Bangui, Ouesso, and Djambala; supplemental Fig. S2). Several hypotheses can be proposed to explain these discrepancies, especially given the fact that SDU is measured with an instrument while cloud reports are performed by observers. Inaccuracies in cloud observations or inconsistencies between observers may be greater when skies are slightly cloudy and/or clouds are broken. The number of daytime cloud-cover observations may also be insufficient to be representative of the day while sunshine duration is an integration over daytime hours.

Second, SDU levels are lower for LCC than for TCC (for the same cloudiness amount). In addition, the dispersion of SDU values for a given cloudiness amount is greater when considering LCC than TCC. These points suggest that 1) low clouds are not the only clouds that reduce incoming solar radiation (if LCC = 4, TCC may vary between 4 and 8 octas) and 2) they are not as good as TCC to match SDU variations, which is expected. Nonetheless low clouds have a particularly strong impact on SDU in JJAS as compared with the other types of clouds as illustrated in Fig. S3 of the online supplemental material. This figure compares SDU levels when the cloud cover (TCC) is dominated by middle and high clouds (LCC < 3octas; Fig.S3a) with those when the cloud cover is dominated by low clouds (LCC = TCC; Fig. S3b). SDU levels are systematically and significantly higher when TCC is mainly composed of low clouds as compared with middle and high clouds. The mean bias evolution along octas classes (not shown) is very subtle, indicating that bias in SARAH-2 does not depend much on the cloud coverage. Overall, the general tendency from this comparison between SDU and cloudiness is that in JJAS SDU can be viewed as a good proxy for the presence of an extensive low-level cloud cover.
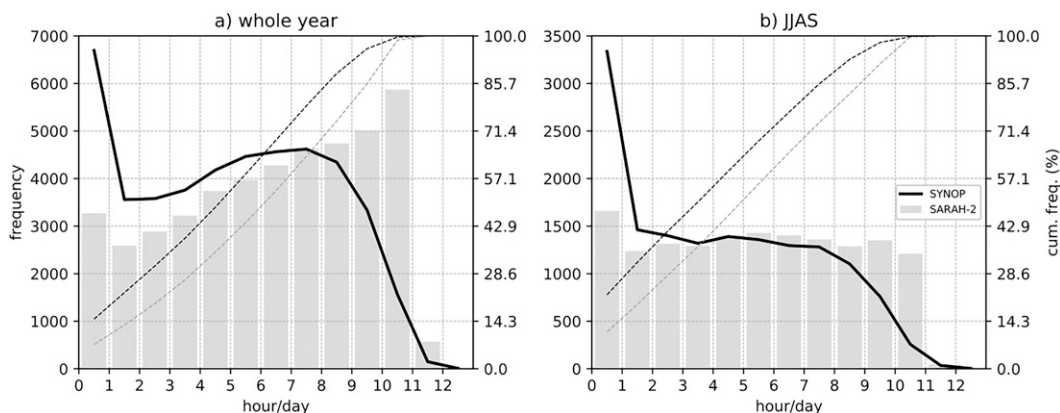

FIG. 11. Distribution of daily sunshine in WEA for (a) the whole year and (b) the June–September cloudy dry season, in SARAH-2 (gray bars) and SYNOP (black curve) for the period 1999–2017. The dashed thin gray and black curves give the cumulative distribution for SARAH-2 and SYNOP, respectively.
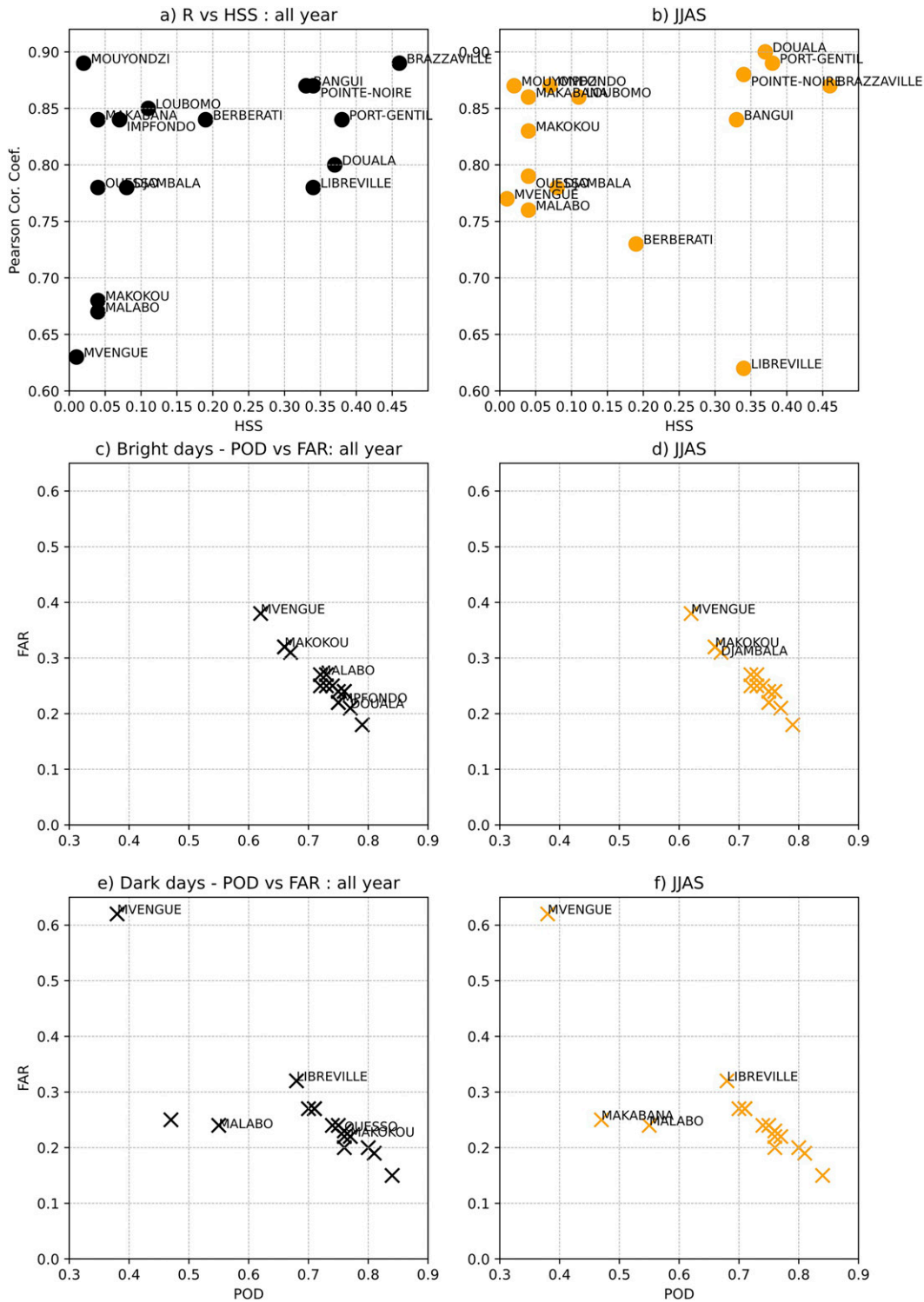
FIG. 12. Scatterplots of HSS and Pearson correlation coefficients for the 16 SYNOP stations retained for analysis for (a) the whole year or (b) the JJAS season only. Scatterplots of POD and FAR scores for (c),(d) dark and (e),(f) bright days considering the whole year in (c) and (e) or the JJAS season only in (d) and (f). The names of stations recording the lowest scores are provided. In (a) and (b), HSS are both for dark and bright days.
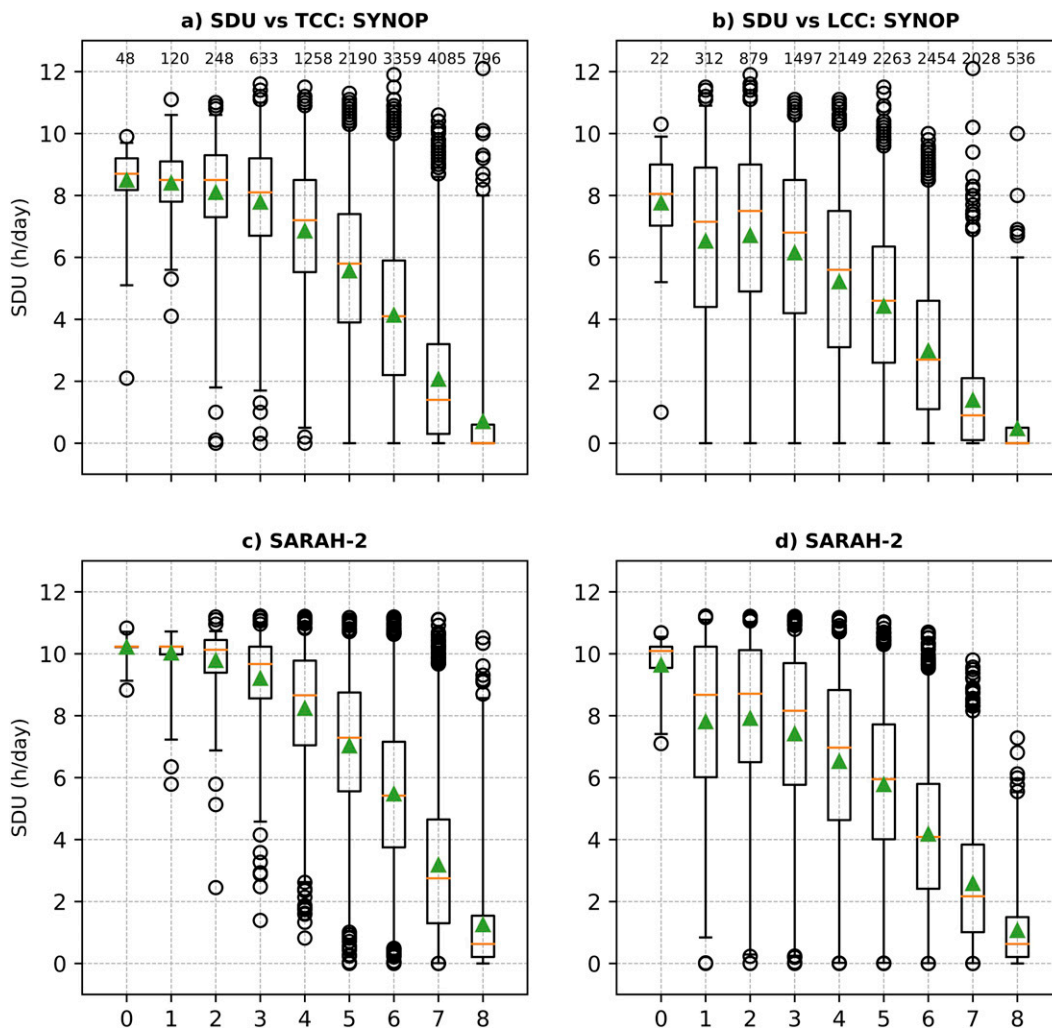
FIG. 13. Boxplots of June–September SDU vs (left) TCC and (right) LCC for (a),(b) SYNOP and (c),(d) SARAH-2 for the period 1999–2017. TCC and LCC records are expressed in octas from 0 for clear skies to 8 for totally overcast skies and come from SYNOP. Boxes extend from the lower to the upper quartile of data, with the median as an orange line. Green triangles give the mean. Circles are outliers beyond the lower or upper quartile divided by the interquartile range (whiskers). The number of available observations (day x station/pixel) by class of cloud cover is given at the top of (a) and (b).

4. Discussion and conclusions

Because of the importance of solar radiation for climate and ecosystems functioning, especially that of the tropical forests, but due to the lack of long-term in situ solar radiation data for WEA, we were led to investigate sunshine duration records. To quantify mean spatial and temporal evolutions of sunshine duration in the course of the annual cycle we jointly analyzed in situ measurements from the FAOCLIM database, SYNOP reports from OGIMET, and satellite estimates provided by CMSAF within the SARAH-2.1 dataset. The good spatial coverage of FAOCLIM complemented by SYNOP reports allowed a much finer characterization of irradiance for WEA than done in previous studies dedicated to SDU in tropical Africa as in Kothe et al. (2017).

On the whole, WEA displays low SDU levels: SDU annual average is around 5 h day^{-1} with the lowest levels at the coast (<4 h day^{-1}) and the highest ones to the southeast and northeast fringes (>6 h day^{-1}). Most stations register minimum levels in July–September and maximum levels in January–March, except the southeasternmost ones, which exhibit an opposite pattern. The July–September low levels of sunshine duration are due to a large cloud fraction—most of the days record a cloud fraction above or equal to 4 octas—mainly resulting from low-level clouds. SDU spatial distribution in July is tightly controlled by topographic features: for instance, the leeward slopes of Mayombé and Batéké Plateaus are 3 times as sunny as the windward slopes. This is likely related to the dominant southwesterly monsoon winds that blow over

the region during this season, combined with a stable low-level troposphere.

While SARAH-2 satellite estimates fairly well reproduce the spatial and seasonal patterns of sunshine duration in WEA, sunshine duration is consistently overestimated. This complements and is in line with results by Kothe et al. (2017) for the neighboring West Africa, CAR, and South Sudan areas. These authors observe a mean annual bias of more than 1.6 h day^{-1} for SARAH-2 for these regions, with the largest bias for the months of September–November. In WEA, there seems to be a tendency for a larger overestimation during the boreal winter months (December–February), especially to the north, which experiences a sunny dry season, than during the boreal summer months (July–September), when most of the region experiences an overcast dry season. Analyses at the daily time scale show that overestimation arises from too few days with SDU levels below 2 h day^{-1}—these days are the most frequent over the region, especially in June–September—and too many days with SDU levels above 9 h day^{-1}.

The suspected reasons for such overestimations are (i) errors in in situ measurements, (ii) determination of the maximum reflectivity in regions with frequent milky skies as WEA, (iii) high-altitude thin clouds, and (iv) thresholds and parameters in algorithms not valid for the region.

Although this cannot account for all the SARAH-2 biases found in this study, in situ sunshine measurements are error prone. Callède and Arquisou (1972) found a difference of 5% between sunshine duration recordings obtained at two nearby locations in Bangui, CAR. According to Iqbal (1983), the reliability of the Campbell–Stokes heliograph, generally used to record sunshine duration, may be affected by the humidity of the recording card. However, the fact that the difference between in situ records and SARAH-2 satellite estimates in WEA are even larger in the boreal winter dry season suggests that this is not a major reason for the discrepancies found in the region.

Milky skies are thought to be particularly common over the region because of high water vapor content due to the proximity of the ocean and transpiration from the underlying dense evergreen forests, and/or aerosols. Aerosol loadings in the WEA atmosphere principally stem from local and neighboring (Angola and CAR) biomass burnings, and are the largest in boreal summer (Liousse et al. 2010; Sayer et al. 2019). But aerosols from Saharan mineral dust have also been traced down to central Africa (Ruellan et al. 1999). Drame et al. (2015) obtained for the neighboring West African region significant improvements in the estimation of incoming solar radiation by considering diurnal variations in both aerosol loads and composition. Actually, aerosol load variations are not explicitly treated in SARAH-2 retrieval, which could also explain biases observed (Neher et al. 2020).

Aerosols would also prevent satellite retrieval from detecting clouds at all, especially the low-level ones. For instance, over the adjacent southeast tropical Atlantic, low clouds lay under the aerosol plumes (LeBlanc et al. 2020), while those inland have a cloud-top temperature close to the ground one. High-altitude thin clouds might also strongly influence satellite estimates more than in situ observations. Dommo et al.

(2018) show that during the June–September season, WEA regularly experiences a high semitransparent cloud coverage: its fraction reaches on average 20%.

In the satellite retrieval used for the generation of the SARAH-2.1 data record, the measured reflectivity is compared with the so-called clear-sky reflectivity, which is derived as the minimum reflectivity throughout the month. In almost all situations the minimum reflectivity corresponds to a clear-sky situation. However, in areas with regular cloud coverage and/or very milky skies as in WEA, no clear-sky situation might be observed from the satellite in several months. In this case, the "clear-sky reflectivity" (i.e., the minimum reflectivity) does not represent clear-sky conditions but "milky"/partly cloudy conditions. As a consequence, the contrast between clouds and the clear-sky reflectivity is reduced, clouds appear too dark and, hence, too thin in retrievals, resulting in an overestimation of surface irradiance and possible sunshine duration. This has also been suggested as the reason for the overestimation of surface solar irradiance in West Africa in the SARAH dataset (Hannak et al. 2017; Kniffka et al. 2019).

In addition, thresholds and parameters values used for the estimation of SDU from DNI might not be appropriate for the region. The actual DNI threshold used in SARAH-2 for bright sunshine equals 120 W m^{-2} following the WMO definition, however, for the surface measurements this threshold may vary from 70 W m^{-2} for a dry climate to 280 W m^{-2} for a very humid climate according to Suehrcke et al. (2013). This raises the question of the comparability of the satellite-based and the surface-measured sunshine duration, even though it is expected that the sunshine duration is only moderately sensitive to the exact value of the threshold radiation. These points definitely require further analysis so that the future versions of SARAH dataset are corrected for these biases for the region.

Because sunshine duration is computed from solar DNI (cf. section 2), our results indicate that solar surface irradiance itself is also overestimated in the SARAH-2.1 dataset for the region. Such an overestimation might be critical for several applications that use these estimations, for instance, the energy sector, but also hydrological and agronomic modeling, climate variability and trends analyses.

The deployment of any solar power plant at a given location requires accurate and precise solar resource assessment at that location (e.g., Yushchenko et al. 2018). Global horizontal irradiance (GHI), which includes both DNI and diffuse horizontal irradiance, is the key value to estimate the final energy yield of a PV project (e.g., Neher et al. 2020). Likewise, DNI is the key value to estimate the final energy yield of a CSP project (Blanc et al. 2014; Hagumimana et al. 2021). Because SDU in this study is calculated from satellite-derived SARAH-2.1 DNI, biases in SDU over WEA point to some extent toward biases in DNI that may result in uncertainty in the power output of the plant and endanger its financial feasibility (or bankability; Polo et al. 2016). Therefore, it would be recommended to apply a site-adaptation procedure to reduce uncertainty in the satellite-based long-term estimates of DNI from SARAH-2.1 by combining them with a short-term ground measurement campaign at the site of the CSP project (Polo et al. 2015; Fernández-Peruchena et al. 2020).

Similarly, SDU and solar radiation are widely used as inputs in crop/vegetation modeling. Bois et al. (2008) note that the propagation of uncertainties in solar radiation estimates at daily time scale can be considerable for solar radiation based ET estimations. Uncertainties in calculated or estimated SDU and SR have also been shown to have significant impacts on yields' simulations (e.g., Wang et al. 2015). Tests should be conducted to assess, for the region, differences obtained in the simulation of ET, yields, and so on when using SDU in situ measurements versus SARAH-2.1 estimates. It would also worth evaluating what would be the added value of interpolating SDU in situ measurements using SARAH-2.1 SDU estimates or converting SDU in situ measurements into GHI with the several existing equations, then interpolating them using SARAH-2.1 (Good 2010). The use of SARAH-2.1 estimates without a bias correction in the agronomic field for the WEA region is expected to lead to too much potential evapotranspiration (and perhaps too-fast phenological cycles).

Last, despite the overestimations observed, skill scores obtained at daily time scale suggest that the time of occurrence of the least sunny and the sunniest days is properly reproduced. Actually, this is promising for studying the intraseasonal and interannual variability of solar radiation over the region. The 35-yr-long historical records offered by SARAH-2.1 (Müller et al. 2015) should allow climate trends detection and analysis, if any, for the region.

Data availability statement. SDU estimates from SARAH-2.1 are openly available from the CMSAF data portal (https://wui.cmsaf.eu/safira/action/viewProduktSearch;jsessionid=4843725FA329F631863F8A5FA966DB25.ku_2). SDU in situ records from FAO were extracted from the FAO-CLIM2 CD-ROM (ordered at http://www.fao.org/nr/climpag/pub/en1102_en.asp). OGIMET SDU in situ records were obtained online (http://www.ogimet.com/index.phtml.en).

REFERENCES

Adole, T., J. Dash, V. Rodriguez-Galiano, and P. M. Atkinson, 2019: Photoperiod controls vegetation phenology across Africa. *Commun. Biol.*, **2**, 391, https://doi.org/10.1038/s42003-019-0636-7.

Amjad, M., M. T. Yilmaz, I. Yucel, and K. K. Yilmaz, 2020: Performance evaluation of satellite- and model-based precipitation products over varying climate and complex topography. *J. Hydrol.*, **584**, 124707, https://doi.org/10.1016/j.jhydrol.2020.124707.

Blanc, P., and Coauthors, 2014: Direct normal irradiance related definitions and applications: The circumsolar issue. *Sol. Energy*, **110**, 561–577, https://doi.org/10.1016/j.solener.2014.10.001.

Bois, B., P. Pieri, C. Van Leeuwen, L. Wald, F. Huard, J. P. Gaudillere, and E. Saur, 2008: Using remotely sensed solar radiation data for reference evapotranspiration estimation at a daily time step. *Agric. For. Meteor.*, **148**, 619–630, https://doi.org/10.1016/j.agrformet.2007.11.005.

Bush, E., and Coauthors, 2020: Ground data confirm warming and drying are at a critical level for forest survival in western equatorial Africa. *PeerJ*, **8**, e8732, https://doi.org/10.7717/peerj.8732.

Callède, J., and G. Arquisou, 1972: Données climatologiques recueillies à la station bioclimatologique de Bangui pendant la période 1963–1971. *Cah. ORSTOM Ser. Hydro.*, **IX**, 3–26.

Cook, K. H., and E. K. Vizy, 2015: The Congo basin Walker circulation: Dynamics and connections to precipitation. *Climate Dyn.*, **47**, 697–717, https://doi.org/10.1007/s00382-015-2864-y.

Dommo, A., N. Philippon, G. Sèze, D. A. Vondou, and R. Eastman, 2018: The June–September low cloud cover in western central Africa: Mean spatial distribution and diurnal evolution, and associated atmospheric dynamics. *J. Climate*, **31**, 9585–9603, https://doi.org/10.1175/JCLI-D-17-0082.1.

Drame, M. S., X. Ceamanos, J. L. Roujean, A. Boone, J. P. Lafore, D. Carrer, and O. Geoffroy, 2015: On the importance of aerosol composition for estimating incoming solar radiation: Focus on the western African stations of Dakar and Niamey during the dry season. *Atmosphere*, **6**, 1608–1632, https://doi.org/10.3390/atmos6111608.

Fernández-Peruchena, C. M., J. Polo, L. Martín, and L. Mazorra, 2020: Site-adaptation of modeled solar radiation data: The SiteAdapt procedure. *Remote Sens.*, **12**, 2127, https://doi.org/10.3390/rs12132127.

Gielen, D., F. Boshell, D. Saygin, M. D. Bazilian, N. Wagner, and R. Gorini, 2019: The role of renewable energy in the global energy transformation. *Energy Strateg. Rev.*, **24**, 38–50, https://doi.org/10.1016/j.esr.2019.01.006.

Gond, V., and Coauthors, 2013: Vegetation structure and greenness in central Africa from Modis multi-temporal data. *Philos. Trans. Roy. Soc.*, **368B**, 20120309, https://doi.org/10.1098/rstb.2012.0309.

Good, E., 2010: Estimating daily sunshine duration over the UK from geostationary satellite data. *Weather*, **65**, 324–328, https://doi.org/10.1002/wea.619.

Guan, K., and Coauthors, 2015: Photosynthetic seasonality of global tropical forests constrained by hydroclimate. *Nat. Geosci.*, **8**, 284–289, https://doi.org/10.1038/ngeo2382.

Hagumimana, N., J. Zheng, G. N. O. Asemota, J. D. D. Niyonteze, W. Nsengiyumva, A. Nduwamungu, and S. Bimenyimana, 2021: Concentrated solar power and photovoltaic systems: A new approach to boost Sustainable Energy for All (Se4all) in Rwanda. *Int. J. Photoenergy*, **2021**, 5515513, https://doi.org/10.1155/2021/5515513.

Hannak, L., P. Knippertz, A. H. Fink, A. Kniffka, and G. Pante, 2017: Why do global climate models struggle to represent low-level clouds in the West African summer monsoon? *J.*

Climate, **30**, 1665–1687, https://doi.org/10.1175/JCLI-D-16-0451.1.

Huete, A. R., and Coauthors, 2006: Amazon rainforests green-up with sunlight in dry season. *Geophys. Res. Lett.*, **33**, L06405, https://doi.org/10.1029/2005GL025583.

Iqbal, M., 1983: *An Introduction to Solar Radiation.* Academic Press, 390 pp.

Kniffka, A., P. Knippertz, and A. H. Fink, 2019: The role of low-level clouds in the West African monsoon system. *Atmos. Chem. Phys.*, **19**, 1623–1647, https://doi.org/10.5194/acp-19-1623-2019.

Kothe, S., U. Pfeifroth, R. Cremer, J. Trentmann, and R. Hollmann, 2017: A satellite-based sunshine duration climate data record for Europe and Africa. *Remote Sens.*, **9**, 429, https://doi.org/10.3390/rs9050429.

Lacaux, J. P., R. Delmas, G. Kouadio, B. Cros, and M. O. Andreae, 1992: Precipitation chemistry in the Mayombé forest of equatorial Africa. *J. Geophys. Res.*, **97**, 6195–6206, https://doi.org/10.1029/91JD00928.

LeBlanc, S. E., and Coauthors, 2020: Above-cloud aerosol optical depth from airborne observations in the southeast Atlantic. *Atmos. Chem. Phys.*, **20**, 1565–1590, https://doi.org/10.5194/acp-20-1565-2020.

Liousse, C., and Coauthors, 2010: Updated African biomass burning emission inventories in the framework of the AMMA-IDAF program, with an evaluation of combustion aerosols. *Atmos. Chem. Phys.*, **10**, 9631–9646, https://doi.org/10.5194/acp-10-9631-2010.

Longandjo, G.-N. T., and M. Rouault, 2020: On the structure of the regional-scale circulation over central Africa: Seasonal evolution, variability and mechanisms. *J. Climate*, **33**, 145–162, https://doi.org/10.1175/JCLI-D-19-0176.1.

Maranan, M., A. H. Fink, and P. Knippertz, 2018: Rainfall types over southern West Africa: Objective identification, climatology and synoptic environment. *Quart. J. Roy. Meteor. Soc.*, **144**, 1628–1648, https://doi.org/10.1002/qj.3345.

Müller, R., U. Pfeifroth, C. Träger-Chatterjee, J. Trentmann, and R. Cremer, 2015: Digging the METEOSAT treasure—3 decades of solar surface radiation. *Remote Sens.*, **7**, 8067–8101, https://doi.org/10.3390/rs70608067.

Myneni, R. B., and Coauthors, 2007: Large seasonal swings in leaf area of Amazon rainforests. *Proc. Natl. Acad. Sci. USA*, **104**, 4820–4823, https://doi.org/10.1073/pnas.0611338104.

Neher, I., S. Crewell, S. Meilinger, U. Pfeifroth, and J. Trentmann, 2020: Photovoltaic power potential in West Africa using long-term satellite data. *Atmos. Chem. Phys.*, **20**, 12 871–12 888, https://doi.org/10.5194/acp-20-12871-2020.

Neupane, N., 2016: The Congo basin zonal overturning circulation. *Adv. Atmos. Sci.*, **33**, 767–782, https://doi.org/10.1007/s00376-015-5190-8.

Philippon, N., and Coauthors, 2016: Analysis of the diurnal cycles for a better understanding of the mean annual cycle of forests greenness in central Africa. *Agric. For. Meteor.*, **223**, 81–94, https://doi.org/10.1016/j.agrformet.2016.04.005.

——, and Coauthors, 2019: The light-deficient climates of western central African evergreen forests. *Environ. Res. Lett.*, **14**, 034007, https://doi.org/10.1088/1748-9326/aaf5d8.

Polo, J., L. Martín, and J. M. Vindel, 2015: Correcting satellite derived DNI with systematic and seasonal deviations: Application to India. *Renewable Energy*, **80**, 238–243, https://doi.org/10.1016/j.renene.2015.02.031.

——, F. M. Téllez, and C. Tapia, 2016: Comparative analysis of long-term solar resource and CSP production for bankability. *Renewable Energy*, **90**, 38–45, https://doi.org/10.1016/j.renene.2015.12.057.

Quansah, D. A., M. S. Adaramola, and L. D. Mensah, 2016: Solar photovoltaics in sub-Saharan Africa—Addressing barriers, unlocking potential. *Energy Proc.*, **106**, 97–110, https://doi.org/10.1016/j.egypro.2016.12.108.

Ruellan, S., H. Cachier, A. Gaudichet, P. Masclet, and J.-P. Lacaux, 1999: Airborne aerosols over central Africa during the Experiment for Regional Sources and Sinks of Oxidants (EXPRESSO). *J. Geophys. Res.*, **104**, 30 673–30 690, https://doi.org/10.1029/1999JD900804.

Sayer, A. M., and Coauthors, 2019: Two decades observing smoke above clouds in the south-eastern Atlantic Ocean: Deep Blue algorithm updates and validation with ORACLES field campaign data. *Atmos. Meas. Tech.*, **12**, 3595–3627, https://doi.org/10.5194/amt-12-3595-2019.

Suehrcke, H., R. S. Bowden, and K. G. T. Hollands, 2013: Relationship between sunshine duration and solar radiation. *Sol. Energy*, **92**, 160–171, https://doi.org/10.1016/j.solener.2013.02.026.

Upadhyaya, H. D., M. Vetriventhan, and V. C. R. Azevedo, 2021: Variation for photoperiod and temperature sensitivity in the global mini core collection of sorghum. *Front. Plant Sci.*, **12**, 571243, https://doi.org/10.3389/fpls.2021.571243.

Verhegghen, A., P. Mayaux, C. De Wasseige, and P. Defourny, 2012: Mapping Congo basin vegetation types from 300 m and 1 km multi-sensor time series for carbon stocks and forest areas estimation. *Biogeosciences*, **9**, 5061–5079, https://doi.org/10.5194/bg-9-5061-2012.

Wagner, F. H., and Coauthors, 2017: Climate drivers of the Amazon forest greening. *PLOS ONE*, **12**, e0180932, https://doi.org/10.1371/journal.pone.0180932.

Wang, J., E. Wang, H. Yin, L. Feng, and Y. Zhao, 2015: Differences between observed and calculated solar radiations and their impact on simulated crop yields. *Field Crops Res.*, **176**, 1–10, https://doi.org/10.1016/j.fcr.2015.02.014.

Wilks, D. S., 2011: *Statistical Methods in the Atmospheric Sciences.* 3rd ed. Elsevier, 675 pp.

World Meteorological Organisation, 1969: Climatological Normals (CLINO) for climate and climate ship stations for the period 1931–1960. WMO Doc. 117, https://community.wmo.int/bookstore/climatological-normals-clino-climat-and-climat-ship-stations-period-1931-1960.

——, 1998: 1961–1990 Global Climate Normals (CLINO), Version 1.0. CD-ROM. WMO Doc. 847, https://community.wmo.int/bookstore/1961-1990-global-climate-normals-clino.

Yang, X., and Coauthors, 2021: A comprehensive framework for seasonal controls of leaf abscission and productivity in evergreen broadleaved tropical and subtropical forests. *Innovation*, **2**, 100154, https://doi.org/10.1016/j.xinn.2021.100154.

Yushchenko, A., A. de Bono, B. Chatenoux, M. K. Patel, and N. Ray, 2018: GIS-based assessment of photovoltaic (PV) and concentrated solar power (CSP) generation potential in West Africa. *Renewable Sustainable Energy Rev.*, **81**, 2088–2103, https://doi.org/10.1016/j.rser.2017.06.021.

Zhou, L., and Coauthors, 2014: Widespread decline of Congo rainforest greenness in the past decade. *Nature*, **509**, 86–90, https://doi.org/10.1038/nature13265.